

# Simultaneous model discovery and state estimation under high data corruption

Teddy Meissner\* and Karl Glasner †

**Abstract.** This paper proposes a sparse regression strategy for discovery of ordinary differential equations from incomplete and noisy data. Inference is performed over both equation parameters and state variables using a statistically motivated likelihood function. Sparsity is enforced by a selection algorithm which iteratively removes terms and compares models using statistical information criteria. Large scale optimization is performed using a second-order variant of the Levenberg-Marquardt method, where the gradient and Hessian are computed via automatic differentiation. The proposed method is illustrated and tested on several systems with varying levels of noisy and incomplete data. Comparisons are made to a state-of-the-art algorithm for system identification, demonstrating competitiveness of the proposed approach.

**Key words.** system identification, sparse regression, inverse problems, differential equations

**MSC codes.** 93B30, 34A55, 35R30

**1. Introduction.** Combining physical laws with observational data is an ongoing scientific challenge. Whereas differential equations derived entirely from first principles have been broadly successful in basic physics and mechanics, this approach is insufficient for complex systems ranging from materials science to biology. In those cases, model development involves a variety of phenomenological assumptions, which must be calibrated or verified from observations. Many recent efforts have focused on the problem of model discovery, which involves generating equations from scratch that attempt to balance trade-offs between fitting data, parsimony, and interpretability of the discovered model.

Historically, the earliest methods of combining data and differential equations were concerned with the inverse problem of parameter estimation (e.g. [55] and references therein). Traditional nonlinear least squares regression (known in various contexts as the shooting method or adjoint method), seeks to minimize only the difference between model output and data (e.g. [22, 2, 4, 24, 31, 16, 53, 64, 77, 26]). An alternative is to optimize over the equation’s residual, the error obtained when the data is inserted into the model. This idea forms the basis for many recent studies of both parameter estimation and model discovery [53, 12, 28, 36, 13, 60]. Methods which simultaneously infer the state and parameter variables (hereafter called “hybrid” regression) interpolate between these two approaches [54, 70, 23, 57, 58, 27], and have proven to be more robust for handling noisy and incomplete data. Gaussian process regression [50, 51] has also been proposed for system identification. Lastly, a variety of studies employ Bayesian inference (e.g. [18, 6, 23, 74, 77, 76]) that can provide a detailed probability distribution of parameter values, which is useful for tasks such as uncertainty quantification.

Discovering differential equations from data, rather than estimation of parameters in a

---

\*Corresponding Author: Program in Applied Mathematics, University of Arizona, Tucson AZ 85721 USA ([tmeissner@arizona.edu](mailto:tmeissner@arizona.edu)).

†Department of Mathematics, University of Arizona, Tucson AZ 85721 USA ([kglasner@arizona.edu](mailto:kglasner@arizona.edu)).

known model, has seen a surge of interest. Some of the earliest work in this direction involves symbolic regression [9, 62]. These procedures consist of generating candidate equations by symbolically combining elementary operations, and testing them competitively to ensure a good fit with the data. A variety of extensions build upon this idea, employing either genetic algorithms or deep learning strategies [38, 69, 5, 43, 14].

An alternative to symbolic discovery involves regression with a given set of candidate terms, or at least a general equation structure. In order to identify models which are both parsimonious and do not overfit data, these methods rely on promoting sparsity in the parameter set. This can be accomplished by using statistical information criteria [41],  $L^1$  penalization [60], or a sequential thresholding algorithm (“SINDy”) [13, 59]. Sparsity has also been incorporated into Bayesian versions of model discovery [10, 30].

It has become increasingly popular to employ neural network function approximation [7, 52] instead of traditional grid-based or finite element representations. These “physics-informed” machine learning methods [32] rely on a loss function similar to hybrid regression methods discussed above, inferring both the solution and parameters. They have been adapted to model discovery by including a sparsity-inducing penalty term in the loss function, and search for equations composed of predefined library terms [11, 72] or represented by rational neural networks [67, 66]. Alternatively, neural networks may be employed to approximate functions that define a dynamic model directly [33, 29, 47].

Despite the proliferation of methods for data-driven model discovery, there are a variety of outstanding challenges. Here we highlight some of these and explain how they are addressed here.

- **Noisy data.** Methods that utilize residual regression, most notably the SINDy algorithm, are very sensitive to noise. Subsequent modifications of the original algorithm address this by direct filtering of the data [61, 71], ensemble techniques which average results using multiple data sets [20, 17], or employ additional sparsity requirements in the data set so as to identify outliers [75]. Another body of work utilizes Galerkin-type weak formulations of the equations [56, 44, 45, 68], which produces the effect of a customized low-pass filter. Our method does not rely on direct or indirect filtering, but rather uses inference to produce a system state which interpolates between the provided data and an exact smooth solution of the differential equation, which is determined simultaneously.
- **Incomplete data.** For practical reasons, observed output values of the model may not be present throughout the domain, or might not be provided for every solution component. This is clearly problematic for residual regression approaches which rely on differentiation of the data itself, although one proposed weak formulation shows promise in handling latent (unmeasured) variables [56]. The hybrid regression approach used here, on the other hand, looks to fit a model with whatever data is available, and can be effective for inference of differential equations using remarkably little information [54, 58, 27].
- **State inference.** In the course of model discovery, one might also want to estimate the true ground state, that is the solution of the actual model. This can in principle be done with any discovery method for which side conditions are known, simply by integrating the discovered system forward in time. This would be problematic in chaotic

systems, however, since even if the exact model were known, solution trajectories are highly sensitive to noise in the initial condition and would diverge from the true state. Our method simultaneously infers both the model and a state which represents an approximate solution to the discovered equations. Our numerical experiments (section 5.2) verify that the ground state solution can be accurately recovered in chaotic systems even in the presence of significant noise.

- **Equations which are nonlinear in parameters.** A typical starting point for model discovery involves choosing a library of candidate terms, and supposing the equations are sparse linear combinations of these terms. This is necessary for methods that rely on residual regression (e.g. SINDy and its variants), since the least squares problem is exactly linear. On the other hand, this assumption is fairly restrictive, and a more general regression method is needed to deal with such cases (see section 5.4).

We employ a formulation that accounts for uncertainties in both the model and data, an idea which has statistical roots in data assimilation [19, 73]. In this framework, ignoring uncertainties in the data leads to (SINDy-type) residual regression [23], which explains why such approaches struggle with noisy data. Conversely, parameter estimation that ignores model uncertainty can be highly non-convex and problematic from an optimization standpoint [55, 27].

Recently, system identification methods have been proposed which take both types of uncertainty into account. This is most commonly done in conjunction with maximum likelihood estimation [54, 70, 58, 27], and results in a hybrid regression method that optimizes over both parameters and state variables. The multiple shooting method of Retzler et al. [57] is a version of this, where only a small subset of state variables are inferred, and the remainder are determined by forward integration. A more elaborate Bayesian setting was utilized by Galioto & Gorodetsky [23], who use an exact likelihood expression that accounts for both types of uncertainty, but leads to computationally expensive integrals that ultimately require Monte Carlo techniques. The maximum likelihood approach was extended to include model sparsity by Ribera et al. [58]. Lastly, sparse system identification using neural networks has been proposed by Nguyen et al. [47] and Stephany and Earls [67, 66]. These works employ a loss function similar in character to the objective in maximum likelihood estimation.

This paper introduces a hybrid sparse regression approach that accounts for data and model uncertainty. It is shown to accurately reconstruct systems of ordinary differential equations in circumstances where the supplied data is both noisy and incomplete. Novel aspects include:

- Sparsity is enforced via Bayesian information criteria, rather than by sweeping over hard threshold values as in [58];
- We demonstrate that a second-order optimization method can be made practical using automatic differentiation and a graph-coloring algorithm that takes advantage of the sparsity of the Hessian matrix. This contrasts to first order optimization methods used elsewhere for system identification [58, 47, 67, 66].
- Extensive numerical experiments are conducted, investigating the proposed method's robustness to high noise and missing data.
- Comparisons of both system recovery rates and parameter estimates are made to the WSINDy algorithm [44], a widely used benchmark for system identification.

- Our approach is formulated with generality in mind. In particular, there is no restriction to equations which are linear in parameters, which is a common drawback to many library-based methods. We provide an example in section 5.4 to illustrate this feature.

This paper is structured as follows. Formulation of our regression strategy and its statistical underpinnings are given in section 2. The sparse selection methodology that leads to an explicit algorithm is discussed in section 3. Details of numerical discretization and optimization methods employed are provided in section 4. Finally, several computational examples and comparisons of model discovery are given in section 5.

**2. Problem formulation.** Suppose that a differential equation is discretized and written in the form

$$(2.1) \quad N(u; \theta) = 0,$$

where  $u \in \mathbb{R}^n$  is the state vector and  $\theta \in \mathbb{R}^p$  encapsulates all the unknown constitutive parameters in the model, which might arise within the equation or side conditions. The function  $N : \mathbb{R}^n \times \mathbb{R}^p \rightarrow \mathbb{R}^n$  is assumed to be a generic, differentiable nonlinear operator. No particular type of discretization (finite difference, finite element, neural network, etc.) is assumed at this stage, only that the approximate solution is described by the vector  $u$ .

Our main interest is to determine a sparse estimate for  $\theta$  inferred from information about the solution, which could be obtained either from physical observation or derived from other computations. This information is supplied in the form of noisy and possibly incomplete data  $\hat{u} \in \mathbb{R}^{\hat{n}}$ , which approximates  $u$  on a subset  $D$  of components. The notation  $v|_D$  will represent restriction of the vector  $v$  to the subset  $D$ .

We begin with the simpler problem of estimation of  $\theta$  without any regard to sparse selection. A classical approach to parameter estimation is maximum likelihood regression, which utilizes a likelihood function determined from a known (or parametric) statistical distribution of data. For example, if the only source of uncertainty is zero-mean Gaussian noise with variance  $\sigma^2$  in the data and  $u^*(\theta)$  represents the exact (and unique) solution for parameters  $\theta$ , the likelihood is the conditional probability

$$(2.2) \quad L(\theta) = (\sigma\sqrt{2\pi})^{-\hat{n}} \exp\left(-\frac{\|\hat{u} - u^*(\theta)|_D\|_2^2}{2\sigma^2}\right).$$

Estimation of  $\theta$  is therefore a nonlinear least squares fitting procedure, obtained by maximizing (2.2).

A more general approach takes into account uncertainty in both the data and the underlying model. For instance,  $N(u; \theta)$  can be regarded as random, obeying a distribution with zero-mean and small variance. Under these assumptions, an approximate log-likelihood function can be written as [27]

$$(2.3) \quad L(\theta) = -\frac{\hat{n}}{2} \ln F(\theta), \quad F(\theta) \equiv \min_u \lambda \|\hat{u} - u|_D\|_2^2 + \|N(u; \theta)\|_2^2.$$

Here  $\lambda$  is a ratio of variances that describes the relative uncertainty in the model compared to the data. Expression (2.3) infers both parameter and solution variables  $\theta$  and  $u$  in the

following sense. Defining

$$(2.4) \quad \mathcal{L}_\lambda(\theta, u) = \|N(u; \theta)\|_2^2 + \lambda \|\hat{u} - u|_D\|_2^2,$$

the maximum likelihood estimate is obtained by minimizing  $\mathcal{L}_\lambda$  over both  $\theta$  and  $u$ .

A brief study of the limiting behavior in (2.4) for small and large  $\lambda$  is illuminating, as we can see that this optimization problem interpolates between two types of regression: nonlinear least squares, and residual-only minimization. For  $\lambda \ll 1$ , the leading order minimization problem involves only the first term in (2.4). This problem is degenerate, and has a family of global minimizers  $u^*(\theta)$  which solve  $N(u^*(\theta), \theta) = 0$ . By expanding the exact minimum  $u_{min} = u^*(\theta) + O(\lambda)$ , a solvability condition is determined at order  $\lambda$ , which involves minimization of  $\|\hat{u} - u^*(\theta)|_D\|_2^2$  over  $\theta$ . This problem is precisely the same as minimizing (2.2), which is the nonlinear least squares solution sought in classical parameter estimation.

In contrast, when  $\lambda \gg 1$ , the second term in (2.4) dominates, and the leading order state variable is  $u \approx \hat{u}$  (assuming no restriction to a subset  $D$  of data). This is again a degenerate situation, as  $\theta$  is not determined at this level of optimization. In this case, the expansion  $u_{min} = \hat{u} + \lambda^{-1}u_1 + \dots$  leads to the correction defined by

$$(2.5) \quad \min_{u_1, \theta} \|N(\hat{u}; \theta)\|_2^2 + \|\hat{u} - u_1\|_2^2.$$

This problem decouples, leading to the residual minimization problem

$$(2.6) \quad \min_{\theta} \|N(\hat{u}; \theta)\|_2^2.$$

This type of regression is at the heart of the SINDy algorithm [13] and its derivatives. From a statistical point of view, this limit ignores uncertainty in the data, which is consistent with the observation that residual regression struggles with noise. Various attempts to improve this situation have been proposed, significantly the weak-SINDy algorithm [44], which we later make empirical comparisons to.

Discovery of equations, as opposed to parameter estimation, must take into account a wide variety of candidate models as well as parameters. Model selection can be performed by insisting on sparsity, that is, selecting a small number of terms which provides a reasonable description of the supplied data. A typical approach is to include a sparsity promoting penalty  $R(\theta)$  in the regression formulation,

$$(2.7) \quad \mathcal{L}_{\lambda, R}(\theta, u) = \|N(u; \theta)\|_2^2 + \lambda \|\hat{u} - u|_D\|_2^2 + R(\theta).$$

Various choices for the penalty function are described in the next section.

**3. Methodology.** The problem setup described in section 2 makes no restriction on the choice of generalized model  $N(u; \theta)$ . Commonly,  $N(\cdot)$  is taken to be a linear combination

$$(3.1) \quad N = N_0(u) + \sum_{k=1}^p \theta_k N_k(u).$$

where  $\{N_k\}$  represent a predetermined library of possible candidates. We will also consider a case (section 5.4) where the library terms themselves have parameter dependence.

A constraining feature of library-based system identification methods (SINDy, etc.) is the need for subjective assumptions about the structure of the system. This could be done using expert knowledge of a scientific application, for example by tailoring them to obey symmetries or underlying physics. More commonly, library terms are specified generically, e.g. as multinomials, which is the approach taken in our numerical studies. While in principle multinomials can approximate functions in a general way, in the spirit of parsimonious modeling it is reasonable to limit their order to a reasonable predefined size.

It is supposed that most terms in (3.1) have no significance in describing the data. One approach to identifying such terms is the addition of a sparsity-inducing penalty as in (2.7). A common choice for  $R(\theta)$  is provided by the “norm”  $\|\theta\|_0$ , which is a simple count of the number of non-zero components. Despite it being the most natural measure of sparsity, it is problematic in optimization, and can lead to intractably high computational complexity. Alternatives include other norms on  $\theta$ , notably  $l_1$  or  $l_2$ , which do not exhibit the same computational difficulties associated with the  $l_0$  penalty, but are known to produce significant bias in parameter estimates.

In our work, we utilize (2.7) as a means to identify candidate terms which may or may not be removed according to an information criteria-based algorithm (see section 3.2). We adopt the regularized  $l_0$  penalty proposed in Mohimani et al. [46]

$$(3.2) \quad \|\theta\|_\epsilon = \sum_{i=1}^d \left( 1 - \exp\left(-\frac{\theta_i^2}{2\epsilon^2}\right) \right),$$

where it is clear that  $\lim_{\epsilon \rightarrow 0} \|\theta\|_\epsilon = \|\theta\|_0$ . This smooth approximation allows for gradient-based optimization methods for (2.7), enabling more practical implementations in high-dimensional settings.

**3.1. Model comparison and subset selection.** Under assumptions of model sparsity, it is necessary to prescribe methods for selecting and comparing different subsets of model terms. The most straightforward approach is to recursively remove terms with parameters below a predefined threshold value (e.g. [13, 59]). Alternatively, accepting the removal of one or more terms may be decided by a different measure. Two well-established model selection tools used in statistical analysis and machine learning are the Akaike Information Criteria (AIC) [3] and the closely-related Bayesian information criteria (BIC) [63]. Both of these seek to balance the goodness of fit of the model with its complexity. The practical difference is that BIC places a higher penalty on models with more parameters, and it is more stringent against overfitting in scenarios with large datasets. We found that empirically, BIC gave somewhat more satisfactory results, and is used in our latter tests.

The Bayesian Information Criterion (BIC) (also known as the Schwarz criterion) is defined as

$$(3.3) \quad \text{BIC} = \ln(n)d - 2 \log L,$$

where  $d$  is the number of parameters in the model and  $L$  is the likelihood of the model given the data. Models with smaller BIC scores are preferred. For our specific likelihood function

(2.3), we therefore seek to minimize

$$(3.4) \quad \text{BIC}(u, \theta) = \ln(\hat{n})\|\theta\|_0 + \hat{n} \ln \left( \|N(u; \theta)\|_2^2 + \lambda \|\hat{u} - u\|_D^2 \right)$$

over both  $u$  and  $\theta$ . In practice, the second term is minimized for models with a specified combination of terms, and the corresponding information criteria scores are used to decide which is best.

**3.2. Model selection algorithm.** Given a library with  $p$  potential terms, there are  $2^p$  subset models, so it is impractical to evaluate the information criteria of the entire set of sparse models. Instead, our aim is to efficiently assess a limited range of possibilities, by selectively removing terms guided by the sparse loss function (2.7), and verifying that (3.4) is reduced at each step. An outline of the algorithm is presented in Algorithm 3.1.

Our method begins with simultaneous minimization of the non-sparse loss  $\mathcal{L}_\lambda$  and the sparse loss  $\mathcal{L}_{\lambda,R}$ . Initial guesses are provided for the first iteration of optimization, and thereafter are provided by previous optimizations. The dual loss functions serve distinct purposes: the unpenalized objective  $\mathcal{L}_\lambda$  provides the likelihood of a model given a specific set of parameters and is used in (3.4), whereas  $\mathcal{L}_{\lambda,R}$  encourages irrelevant terms to be small, so they can be targeted for removal.

The algorithm begins with all terms in the model library, and selects an initial number  $k = k_0$  of terms which will be removed at each iteration, provided that (3.4) decreases. If this is not the case, the algorithm reverts to the best model so far and reduces  $k$  to one for small refinements around the current best model. If further steps are accepted, the process continues in the *forward* refinement stage until (3.4) increases, at which point the algorithm terminates (see figure 1, left). Alternatively, if pruning a single parameter from the best model leads to rejection just after  $k$  is reduced, the algorithm assumes that too many terms in the previous step were removed. This triggers the *backwards* refinement stage (see figure 1, right). Here, the algorithm iteratively adds one term back into the model at a time, until the information criteria no longer decreases. To determine which terms to add back in, we revert to the model which has  $k_0$  more terms than the best model, that is, the iteration just prior to the current minimum. From here, pruning  $k_0 - 1$  terms is equivalent to adding one term back into the current model. The process continues by adding one term back at a time until no improvements are found. The algorithm requires at most  $\lceil \frac{p}{k_0} \rceil + k_0 + 1$  iterations, where  $\lceil \cdot \rceil$  denotes the ceiling function.

We can provide a heuristic argument about the convergence of the algorithm to the true minimum of (3.4). Define

$$B(n) = \min_{u, \theta, \|\theta\|_0 = n} \text{BIC}(u, \theta),$$

where  $n$  is less than or equal to the maximum number of library terms. It follows that the minimum we seek is simply  $\min_n B(n)$ . At each step of the algorithm, we have a model with  $n$  terms, and a corresponding value of (3.4) we can call  $\tilde{B}(n)$ . Provided  $\tilde{B}(n)$  is an accurate reflection of  $B(n)$ , minimizing  $\tilde{B}(n)$  over  $n$  would be sufficient. Note that whether the algorithm finishes in the forward or backward stage, the termination conditions are  $\tilde{B}(n-1) \geq \tilde{B}(n^*)$  and  $\tilde{B}(n+1) \geq \tilde{B}(n^*)$ , assuming the final number of terms  $n^*$  is strictly less than the

library size. If  $B(n)$  is well approximated by  $\tilde{B}(n)$ , then the termination conditions guarantee that the desired minimum is recovered.

This approach is designed not only to identify the most parsimonious model, but also to methodically explore and document the performance of various models. Each tested model, along with its corresponding information criterion scores, is recorded, allowing for a comprehensive analysis. This strategy ensures that the search space is efficiently explored, increasing the likelihood of identifying the most effective model configuration.

---

**Algorithm 3.1** Adaptive Pruning with Forward Refinement and Backward Recovery
 

---

**Require:** Initial model  $(u_0, \theta_0)$ , block size  $k$ , data and sparsity weights  $(\lambda, R)$

```

1: mask  $M' = \mathbf{1}$  ▷ Binary Mask
2: mode  $\leftarrow$  forward, Adaptive  $\leftarrow$  True ▷ Toggle variables for stepwise selection
3:  $(u^*, \theta^*, M^*, IC^*) \leftarrow (u_0, \theta_0, M', \infty)$ 
4:
5: while True do
6:   in parallel:
7:     Solve  $(u', \theta') \leftarrow \arg \min \mathcal{L}_\lambda(u, \theta \odot M')$ 
8:     Solve  $(u^\dagger, \theta^\dagger) \leftarrow \arg \min \mathcal{L}_{\lambda, R}(u, \theta \odot M')$ 
9:    $IC' \leftarrow \text{BIC}(u', \theta')$ 
10:  if  $IC' < IC^*$  then
11:    Accept:  $(u^*, \theta^*, M^*, IC^*) \leftarrow (M', u', \theta', IC')$ 
12:    if (Adaptive=True) $\wedge$ ( $k = 1$ ) then Adaptive  $\leftarrow$  False ▷ No backward refinement needed
13:  else
14:    if (Adaptive = True) $\wedge$ ( $k > 1$ ) then
15:      Reduce step:  $k \leftarrow 1$  ▷ Try fine forward pruning
16:    else if (Adaptive=True) $\wedge$ ( $k = 1$ ) then
17:      mode  $\leftarrow$  backward ▷ Try fine backward pruning
18:      Adaptive  $\leftarrow$  False
19:    else
20:      break
21:     $M' \leftarrow \text{UPDATEMASK}(\theta^\dagger, M^*, k, \text{mode})$ 
22:  return  $(u^*, \theta^*, M^*)$ 
23:
24: function UPDATEMASK( $\theta^\dagger, M^*, k, \text{mode}$ )
25:  if mode = forward then
26:    Remove  $k$  smallest terms in  $\theta^\dagger$  not already masked
27:  else
28:    Add back  $k$  largest terms previously masked
29:  return new mask  $M'$ 

```

---

**3.3. Hyperparameter selection.** The optimization problem in Algorithm (3.1) depends on three parameters:

- $k_0$ , which defines how many terms to prune each iteration,
- $\lambda$ , which weights the fidelity to observed data, and
- $R$ , which promotes sparsity in the parameter vector  $\theta$ ,

In this work we set  $k_0 = 5$  for simplicity. We found this value to work well on a wide variety of problems, though we note tuning  $k_0$  empirically had very little influence on the discovered model. Rather, it can be tuned based on the size of the library to influence fewer pruning updates.

To determine the best  $(\lambda, R)$  pair, we use a cross-validation approach to find the weights which minimize the generalization error. We split the data into two sets  $D$  and  $V$ , where the former is used for optimization, and the latter for validation. Selection of  $\lambda$  and  $R$  is

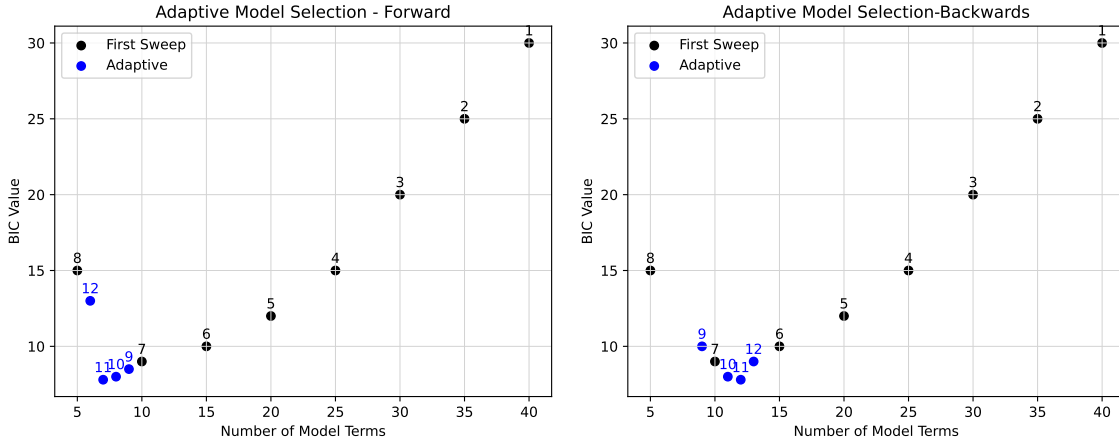


**Figure 1.** Visualization of subset selection methodology to hone in on the correct terms under two different scenarios with parameter drop count  $k = 5$ . Iteration numbers are shown above each point, while both cases show the first model is rejected in iteration 8. Left shows acceptance of small forward steps resulting in no need to go to more complex models. Right shows a small forward step is rejected, resulting in the need for backward steps or testing more complex models.

determined by

$$(3.5) \quad \min_{\lambda, R} \sum_{i \in V} (\hat{u}_i - u_i)^2 \quad \text{s.t. } u \text{ solves Alg. 3.1 on } D$$

In practice, we find that a wide range of hyperparameters prove satisfactory. We therefore enlist a simple grid search over a discrete set of candidate values. For each pair  $(\lambda, R)$ , the inner optimization problem is solved using Algorithm 3.1, and the resulting model is evaluated with a fixed validation set. Figure 2 presents a typical sweep over  $\lambda$  values with  $R$  held fixed, showing the validation error and relative  $\ell_2$  error in the recovered coefficients compared to the ground truth, across varying noise levels. These results are based on the Lorenz system described in section 5.2. While we display only  $\lambda$  dependence in the figure, our full analysis tests combinations of both  $\lambda$  and  $R$ . We see that the validation error and coefficient error tend to reach their minima at similar  $\lambda$  values. This agreement indicates that minimizing validation error is an effective strategy for selecting models that not only generalize well but also recover accurate dynamics.

**3.4. Implementation.** We are interested in discovery of ordinary differential systems

$$(3.6) \quad N(u; \theta) = \frac{du}{dt} - f(u; \theta) = 0,$$

where  $u(t) : \mathbb{R} \rightarrow \mathbb{R}^d$ . In the context of the sparse regression formulation,  $N_0(u) \equiv \frac{d}{dt}u$  and

$$(3.7) \quad N(u; \theta) = N_0(u) - \sum_{k=1}^p \theta_k N_k(u),$$

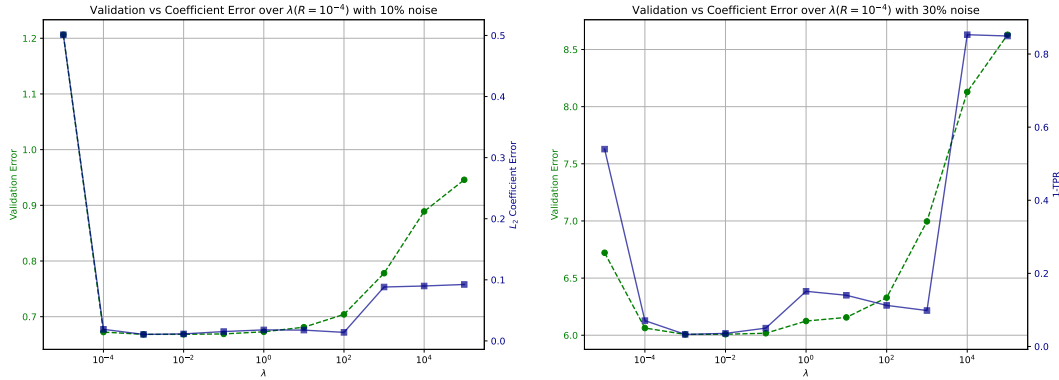


**Figure 2.** Validation error and relative  $l_2$  error in the recovered coefficients for the Lorenz system under 10% noise (left) and 30% noise (right).

where the linear combination of library terms has been identified with  $f(u; \theta)$ . In practice, the state variable  $u(t)$  is represented by some finite dimensional approximation, and the time derivative is replaced with a numerical discretization formula. It is also supposed that data  $\{\hat{u}_i\}$  is provided at times  $\hat{t}_1, \hat{t}_2, \dots, \hat{t}_n$ .

The simplest way to represent the state variable is to consider values  $u_i = u(t_i)$  only at sampling times  $\{\hat{t}_i\}$ . On the other hand, if a more accurate inference of the state is required, one could either determine the state from integration of the inferred system, or a finer grid for values of  $u(t)$  can be employed. The former case leads to integration of an approximate system with approximate initial data, which can be wildly unstable; this problem has been well studied for multiple shooting methods [8]. In the latter case, determining the appropriate grid size for  $u(t)$  might require refinement studies, or analytic error bounds, if they are available. For comparisons of our approach to WSINDy and investigations of incomplete data, we suppose that the given data is sampled (aside from missing regions) at an acceptably fine scale which is used to construct the computational grid. We alternatively study the effect of different computational grid sizes in relation to sampling rates (section 5.5).

Given a computational grid  $\{t_i\}$ , a general class of discretizations of the system (3.7) can be written

$$N_{i+\frac{1}{2}} \equiv \frac{u_{i+1} - I(u_i, \theta, \Delta t_i)}{\Delta t_i} = 0, \quad \Delta t_i \equiv t_{i+1} - t_i,$$

where  $I$  is an integrator of choice using  $u_i$  as the initial condition. We have found that the second-order midpoint method

$$(3.8) \quad N_{i+\frac{1}{2}}(\theta) = \frac{u_{i+1} - u_i}{t_{i+1} - t_i} - f\left(\frac{u_{i+1} + u_i}{2}, \theta\right) = 0, \quad i = 1, \dots, n-1,$$

provides a good trade-off between accuracy and simplicity.

The data error term in (2.4) requires that  $\{t_i\}$  includes a subset of values  $\{t_i | i \in D\}$  where the data is measured. This is accomplished here by simply including the sampling times  $D$  in the discretized grid. A reasonable alternative which is not investigated in this work is to interpolate state values onto the set  $D$ .

With the discretization described above, the loss function  $\mathcal{L}_{\lambda,R}(\theta, u)$  reads

$$(3.9) \quad \mathcal{L}_{\lambda,R}(\theta, u) = \underbrace{\frac{1}{n} \sum_{i=1}^{n-1} N_{i+\frac{1}{2}}(\theta)^2}_{\text{Model Error}} + \underbrace{\frac{\lambda}{\hat{n}} \sum_{i \in D} (\hat{u}_i - u_i)^2}_{\text{Data Error}} + \underbrace{\frac{R}{k} \sum_{i=1}^k \left(1 - \exp\left(-\frac{\theta_k^2}{2\epsilon^2}\right)\right)}_{\text{Sparsity Penalty}},$$

where  $D$  is the set of indices in the domain at which data is available. Components of the ODE system can be written as  $\{x_1, x_2, \dots, x_n\}$ , and a typical model library might look like

$$(3.10) \quad N = \begin{bmatrix} \dot{x}_1 \\ \dot{x}_2 \\ \vdots \\ \dot{x}_n \end{bmatrix} - \begin{bmatrix} x_1 & x_2 & x_1x_2 & x_1x_n & \cdots \\ x_1 & x_2 & x_1x_2 & x_1x_n & \cdots \\ \vdots & \vdots & \vdots & \vdots & \\ x_1 & x_2 & x_1x_2 & x_1x_n & \cdots \end{bmatrix} \circ \theta,$$

where  $M \circ \theta$  denotes the element-wise Hadamard product of a matrix  $M$  and parameter matrix  $\theta$ , followed by summation over rows.

**4. Optimization.** The loss functions described in equations (2.4) and (2.7) are high-dimensional and generally non-convex, posing significant challenges to optimization. A wide variety of methods were investigated here, and we found empirically that a generalized version of the Levenberg-Marquardt (LM) method using the exact Hessian had good performance (see section 4.2).

The original LM algorithm [35, 42] was developed strictly for least-squares problems, and approximates the Hessian using a product of Jacobian matrices akin to the Gauss-Newton method. We employ a more general version that uses the true Hessian [48], which essentially interpolates between gradient descent and Newton’s method. The precise details used in this paper are given in Appendix B.

The main computational effort here involves constructing the Hessian  $H(x)$  and solving for the step  $d_k$  by  $H_\alpha d_k = -g$ , where  $H_\alpha = H + \alpha I$  is the modified Hessian and  $g$  is the gradient. The parameter  $\alpha$  is adjusted adaptively to ensure that a local minimum is found. In the proposed framework, the true Hessian is very sparse, allowing for efficient construction, detailed in section 4.1. The time complexity is therefore dominated by the linear algebra. In this work, the linear solve for  $d_k$  uses sparse Cholesky factorization, while we note for very large problems the conjugate gradient (CG) method may become a more suitable method.

**4.1. Computing the sparse Hessian.** In high-dimensional settings, efficient computation of the objective’s Hessian matrix is a fundamental challenge. Our approach benefits from sparsity that stems from the model’s discretization, however, which makes second-order optimization feasible. The loss functions are compatible with automatic differentiation, which simplifies construction of the Hessian across various applications. To effectively integrate sparsity and automatic differentiation, we first identify the sparsity structure of the Hessian, and subsequently apply graph coloring techniques to minimize the number of Hessian-vector products (HVPs) needed to compute the entire matrix.

**4.1.1. Finding the matrix structure.** To identify the sparsity pattern of the Hessian, we analyze the loss function in its discrete form given in (3.9). Considering each of the three components as independent functions, it is clear the data error and sparse penalty terms have no dependence on neighbor interactions, resulting in a contribution to the Hessian matrix only along the diagonal. Derivatives of the form

$$(4.1) \quad \frac{\partial^2 \|N(u; \theta)\|_2^2}{\partial u_m \partial \theta_n}$$

are generally all non-zero, which creates a dense but small portion of the Hessian that is computed directly.

The largest portion of the Hessian corresponds to state derivatives,

$$(4.2) \quad \frac{\partial^2 \|N(u; \theta)\|_2^2}{\partial u_m \partial u_n} = \sum_{i, j \in N(m) \cap N(n)} \frac{\partial^2 N(u_i; \theta)^2}{\partial u_i \partial u_j}.$$

where  $N(x)$  denotes the neighbors connected at the  $x^{\text{th}}$  grid point. This relationship is provided by the finite difference stencils, which are known in advance and only computed once. The neighbor relation can also be associated with a graph with vertices labeled  $1, 2, \dots, n$  with edges of the form  $(i, N(i))$ . The non-zero contributions in (4.2) can be efficiently computed using graph coloring techniques, as explained next.

**4.1.2. Graph coloring and Hessian vector products.** The Hessian-vector product of a function  $f$  and vector  $v \in \mathbb{R}^n$ , is

$$Hv = \nabla^2 f(x)v = \nabla[\nabla f(x) \cdot v] = \nabla g(x), \quad g(x) \equiv \nabla f(x) \cdot v$$

Computing this involves automatic differentiation to find the gradient of the scalar function  $g$ , rather than directly computing the Hessian of  $f$ . The computational complexity in calculating a dense Hessian is comparable to computing the HVP over all  $n$  coordinate vectors. On the other hand, for sparse matrices, we need to obtain only a small set of binary vectors  $d_1, d_2, \dots, d_k$ , such that  $Hd_1, Hd_2, \dots, Hd_k$  determine  $H$  entirely. Finding a minimal set of such vectors can be reformulated as a graph coloring problem, and particularly for symmetric matrices, a star coloring problem [25]. In contrast to usual graph coloring, star coloring requires every path of length three to use three distinct colors. Vectors  $d_j$  are constructed so their non-zero components are those with color  $j$ , and the non-zero components of the HVP  $Hd_j$  correspond to a subset of Hessian matrix entries. Star coloring is an NP-hard problem, so in practice we utilize an approximate star coloring algorithm [15, 49] which has nearly optimal performance.

**4.2. Numerical Comparison of Algorithms.** To motivate our choice of method, we illustrate the behavior of several first- and second order algorithms. These include L-BFGS, a limited-memory quasi-Newton method [37], nonlinear conjugate gradients [21], trust region newton conjugate gradient method (trust-ncg)[65], trust-krylov, a trust-region method using Krylov subspace approximations, and AdaBelief [78], an adaptive optimizer originally developed for neural networks.

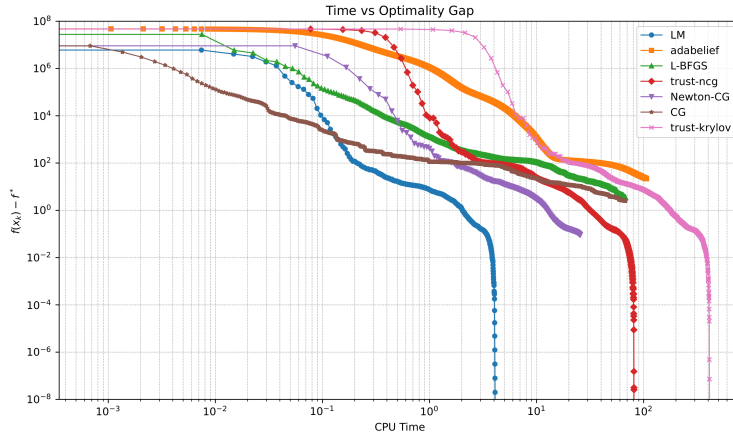


**Figure 3.** Comparison of CPU time (seconds) between the proposed LM method and other standard optimization algorithms.

Our tests use the objective for the problem described in section 5.2, for parameters  $(\lambda, R) = (10^{-2}, 10^{-4})$ . Figure 3 shows CPU time versus the objective function for each method. In this case, the generalized LM method converges at least 10 times faster than the other algorithms tested. In addition, all methods converge to the same local minimum. While we cannot claim that the method we choose would be superior in all settings, it appears to provide reliable performance for all of the test problems discussed next.

**5. Results.** Our system identification algorithm was tested with several well-known model differential equations. Synthetic data were generated using an adaptive Runge–Kutta (4,5) method (RK45) with absolute and relative tolerances of  $10^{-12}$ , and sampled at uniform intervals corresponding to the sampling rates specified in each example. Various amounts of normally distributed noise were added according to

$$\hat{u}_i = u_i^* + \mathcal{N}(0, \sigma^2), \quad \sigma = (\% \text{ noise}) \times \text{standard deviation of } u_i^*,$$

where  $u^*$  denotes noise-free simulation data. We also investigated the effects of incomplete data, by either removing continuous regions (see section 5.1), or removing data randomly (see section 5.2). Note that the latter case could equivalently represent non-uniform data.

To generate reliable initial states for optimization, we linearly interpolate missing state values, but otherwise perform no further pre-processing. To initialize parameters we set  $\theta_k = 1$  and normalize the library functions by setting  $\tilde{N}_k(u) = N_k(u) / \|N_k(\hat{u})\|_2$ , ensuring that each term is initially scaled to a comparable magnitude before optimization. All results are obtained using a grid search over regularization weights  $(\lambda, R) = (10^i, 10^j)$  with  $i \in \{-3, -2, \dots, 3\}$  and  $j \in \{-4, -3, \dots, 0\}$ , resulting in 35 candidate models. For validation, we masked out every third time step, which was used to find the best regularization weight pair as described in section 3.3.

Evaluation of system identification methods is performed using both measures of the accuracy of fit and the success rate in identifying the model structure. The first category of

metrics uses the relative parameter and state errors

$$(5.1) \quad RE(\theta) = \frac{\|\theta - \theta^*\|_F}{\|\theta^*\|_F}, \quad RE(u) = \frac{\|u - u^*\|_F}{\|u^*\|_F}.$$

where  $\|\cdot\|$  is the Frobenius norm and  $\theta^*, u^*$  are the known ground truth parameters and states. A measure of the ability to correctly identify terms is given by the true positivity ratio [34, 45]

$$(5.2) \quad \text{TPR}(\theta) = \frac{\text{TP}}{\text{TP} + \text{FN} + \text{FP}}.$$

Here, TP denotes the number of active terms which are correctly identified, FN is the number of terms incorrectly set to zero, and FP is the number of terms which are incorrectly nonzero.

Our approach is compared to the popular WSINDy method [45], which performs sparse regression on a weak form of the equations. WSINDy utilizes a predefined library of candidate equation terms as we do here, and to date offers some of the best performance for sparse model discovery with highly noisy data. The results presented utilize publicly available codes for WSINDy [45], used here without any customizations.

Having a sufficiently rich library of terms based on expert knowledge or known properties like symmetries would be typical in practice, but is not always available. In our experiments, we provide candidate libraries composed of polynomial terms, up to some predefined order. In the following examples, the true model terms are a subset of our provided libraries; we explore the consequences of insufficient libraries in Appendix A.

All data and codes used in this manuscript are publicly available on GitHub at <https://github.com/TeddyMeissner/DEDi>.

### 5.1. Van der Pol Oscillator.

The Van der Pol system

$$(5.3) \quad \begin{aligned} \dot{x} &= y, \\ \dot{y} &= \mu(1 - x^2)y - x, \end{aligned}$$

arising from a model of electrical circuits, is a non-conservative oscillator with non-linear damping. It is widely used in system identification and nonlinear dynamics studies, offering a classic example of limit cycle behavior and self-sustained oscillations.

To generate data, we used  $\mu = 2$  and initial condition  $(x_0, y_0) = (0, 2)$ . Simulations were performed over the interval  $t \in (0, 10)$ , and the resulting trajectories were sampled at uniform intervals of  $\Delta t = 0.02$ , resulting in a total of 1002 data points across 501 time steps.

We report results using a polynomial library of degree  $p = 3$  and  $p = 6$ . For  $p = 3$ , the library is

$$N = \begin{bmatrix} \dot{x}_1 \\ \dot{x}_2 \end{bmatrix} - \begin{bmatrix} x_1 & x_2 & x_1x_2 & x_1^2 & x_2^2 & x_1^2x_2 & x_1x_2^2 & x_1^3 & x_2^3 \\ x_1 & x_2 & x_1x_2 & x_1^2 & x_2^2 & x_1^2x_2 & x_1x_2^2 & x_1^3 & x_2^3 \end{bmatrix} \circ \theta,$$

where  $\theta \in \mathbb{R}^{2 \times 9}$  contains 18 coefficients to be optimized while  $p = 6$  results in 54 coefficients.

Figure 4 shows a comparison between our approach and WSINDy using boxplots of relative parameter error  $RE(\theta)$  and true positive rate (TPR) across 50 independent noise realizations

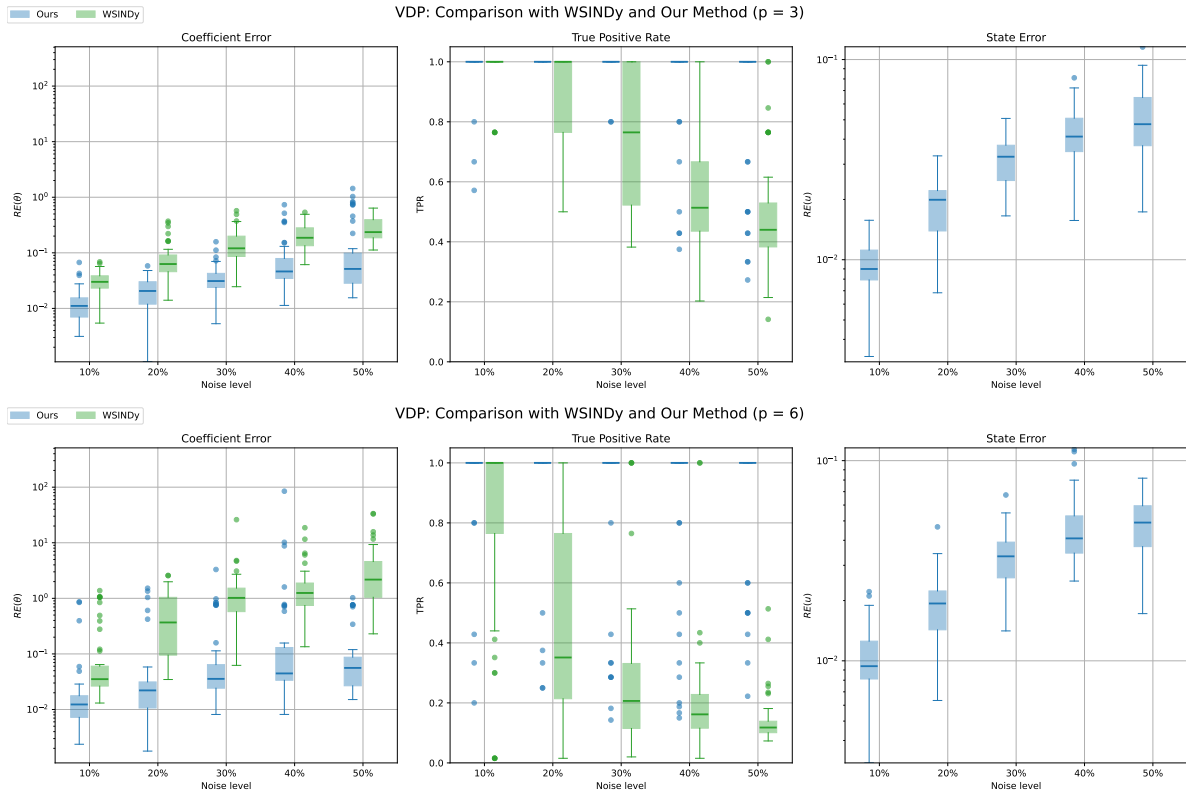


**Figure 4.** Comparison of our algorithm vs. WSINDy for the Van der Pol system, for monomial libraries with maximum orders  $p = 3, 6$  with 18 and 54 terms, respectively. Each boxplot summarizes 50 independent noise realizations per noise level. A line at  $TPR = 1$  indicates that most realizations achieve perfect recovery for our method.

at each noise level. For each boxplot, the central line denotes the median, the box spans the interquartile range (25th–75th percentile), the whiskers extend to the most extreme non-outlier values, and individual points beyond the whiskers represent outliers.

We note our approach consistently outperforms WSINDy across all noise levels, most notably at high noise. In addition, these results demonstrate that our method remains effective when applied to a larger candidate library. The state recovery error  $RE(u)$  (which cannot be compared directly to WSINDy without integration of its discovered system), remains remarkably small despite large observation noise.

A more extreme scenario with both measurement noise and continuous gaps in the observations was considered using a polynomial library of degree  $p = 3$ . (see figure 5). The data shown here sampled at  $\Delta t = .04$ , and data between  $t \in (4, 6)$  are completely removed. This results in a total of 402 data points across 201 time steps. Figure 6 shows boxplots of relative parameter error and true positive rate across 50 samples at varying levels of noise. These results emphasize the robustness of our method under challenging conditions.

Although the system’s structure can usually be determined, occasionally spurious terms appear, mostly at high noise levels. At 10% noise, only two in fifty trials misidentifies model

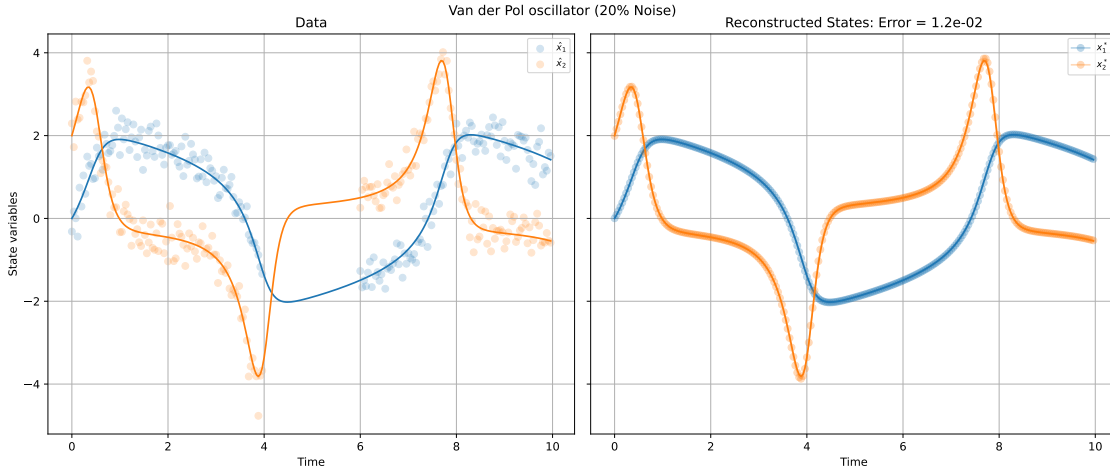


**Figure 5.** Visualization of the Van der Pol oscillator with a missing continuous region of data. Left: the true state of the system (solid), and observed data (dots); Right: the reconstructed state variables.

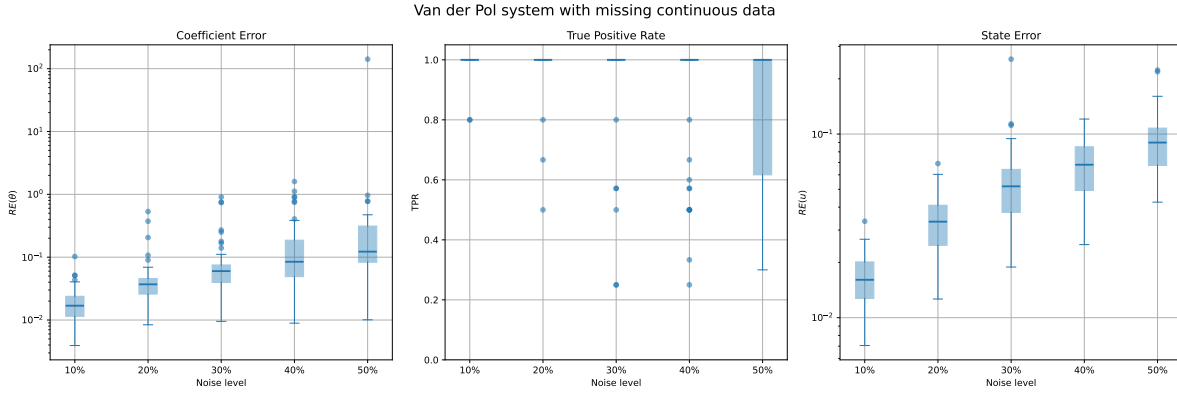


**Figure 6.** Each boxplot summarizes 50 independent noise realizations per noise level for the VDP system with missing continuous data.

terms, and a typical failure mode is provided by the following example:

$$\begin{aligned}\dot{x} &= 1.02y + .03x, \\ \dot{y} &= -1.13x + 2.00y - 2.09x^2y,\end{aligned}$$

which contains an extra, but fairly negligible, term. At 50% noise, 33 out of 50 results were structurally correct, although more severe misidentification problems are occasionally seen. For instance, in one situation the algorithm prematurely discarded a key term, leading to

$$\begin{aligned}\dot{x} &= 1.05y, \\ \dot{y} &= 2.13y - 1.48x^2y - 0.19y^3 - 0.25xy^2.\end{aligned}$$

Despite this, the method consistently captures the core dynamics across most trials, even in the presence of substantial data loss and noise, highlighting its robustness and reliability.

**5.2. The Lorenz system.** The Lorenz equations [40]

$$(5.4) \quad \begin{aligned} \dot{x} &= \sigma(y - x) \\ \dot{y} &= x(\rho - z) + y \\ \dot{z} &= xy - \beta y \end{aligned}$$

were originally derived from models of atmospheric convection, and have become the standard example of chaotic behavior in ordinary differential equations. They have also emerged as a canonical test case in studies of system identification due to their deterministic yet complex behavior.

Simulations used  $(\sigma, \rho, \beta) = (10, 28, 8/3)$  and initial conditions  $(x_0, y_0, z_0) = (-8, 8, 27)$ . The system was simulated over the interval  $t \in (0, 10)$ , and trajectories were sampled at uniform intervals of  $\Delta \hat{t} = 0.02$ , resulting in a total of 1503 data points across 501 time steps. The library of equation terms consisted of monomials up to degree  $p = 3$  and  $p = 4$ . For  $p = 3$ , the library is

$$N = \begin{bmatrix} \dot{x}_1 \\ \dot{x}_2 \\ \dot{x}_3 \end{bmatrix} - \begin{bmatrix} x_1 & \cdots & x_1 x_2 & \cdots & x_3^2 & x_1 x_2 x_3 & \cdots & x_3^3 \\ x_1 & \cdots & x_1 x_2 & \cdots & x_3^2 & x_1 x_2 x_3 & \cdots & x_3^3 \\ x_1 & \cdots & x_1 x_2 & \cdots & x_3^2 & x_1 x_2 x_3 & \cdots & x_3^3 \end{bmatrix} \circ \theta,$$

where  $\theta \in \mathbb{R}^{3 \times 19}$  is a coefficient matrix containing 57 entries. For  $p = 4$ , the resulting library contains 102 terms.

In figure 7, we again benchmark our approach using boxplots of relative parameter errors and recovery rates across 50 independent realizations for each noise level. The results are similar to the previous example, with both better parameter estimates and recovery rates compared to WSINDy. Even with 50% noise, it was often possible to recover an accurate representation of the ground truth model.

To assess performance under incomplete observations, we added 20% noise and randomly removed data points from each state component. Results were performed with a polynomial library of degree  $p = 3$ . Figure 8 presents a representative case with 30% missing data, demonstrating strong agreement between the recovered and true state trajectories. Figure 9 shows the resulting parameter and state errors, along with the recovery rates. For even large quantities of missing data, model parameters can be estimated with good accuracy.

**5.3. The Lorenz-96 system.** To evaluate our method for higher dimensional systems, we utilized the Lorenz-96 model [39], which also exhibits chaotic dynamics, and is often invoked to evaluate data-driven methods for dynamical systems.

For model dimension  $N = 5$ , the dynamics are governed by

$$(5.5) \quad \dot{x}_i = (x_{i+1} - x_{i-2})x_{i-1} - x_i + F, \quad i = 1, \dots, 5.$$

A standard forcing value of  $F = 8$  is used in our simulations with an initial condition slightly perturbed from the equilibrium state  $x(0) = (F+0.01, F, F, F, F)$ . Simulations were performed over the interval  $t \in (0, 10)$  with sampling rate  $\Delta \hat{t} = 0.04$ , resulting in a total of 1255 data points across 251 time steps.

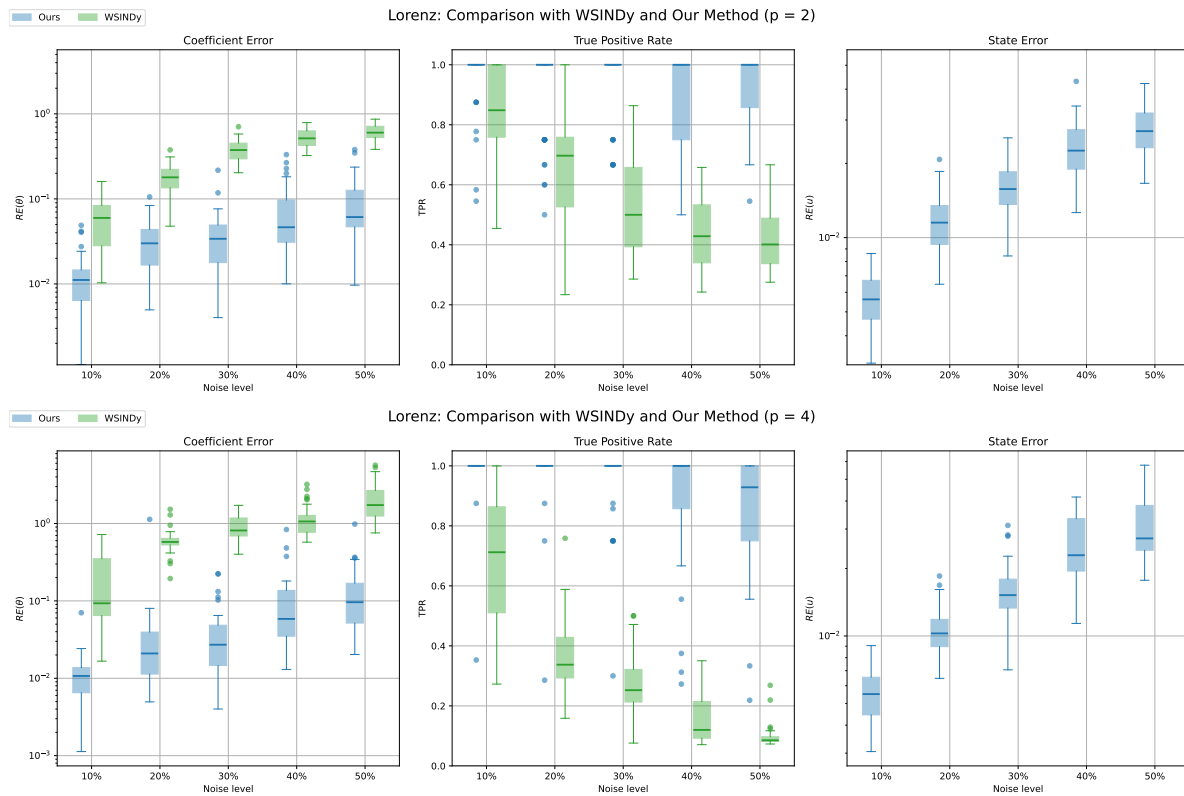


**Figure 7.** Comparison of our algorithm vs. *WSINDy* for the Lorenz system, for monomial libraries with maximum degrees  $p = 3, 4$  with 57 and 102 terms, respectively. Each boxplot summarizes 50 independent noise realizations per noise level.

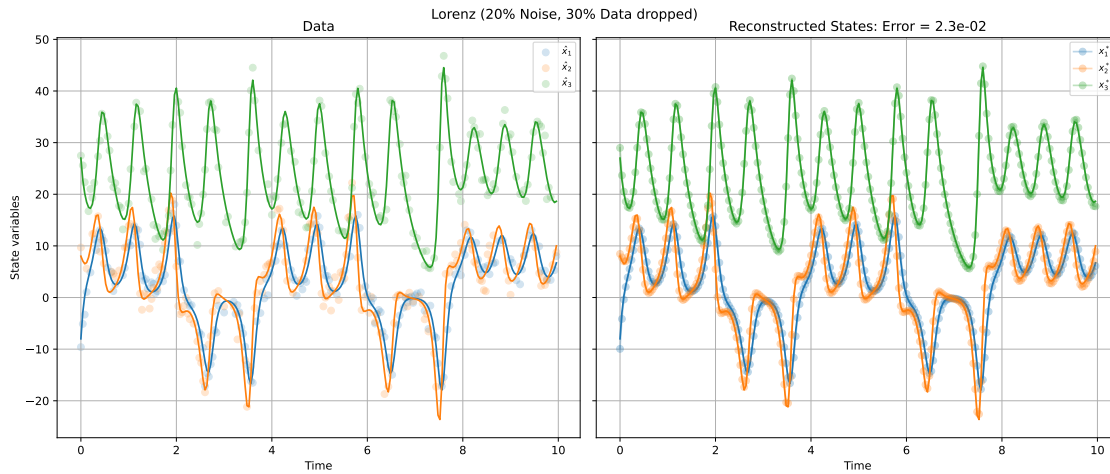


**Figure 8.** Visualization of the Lorenz system with 20% noise and 30% randomly dropped data. Left: the true state of the system (solid), and observed data (dots); Right: the reconstructed state variables.

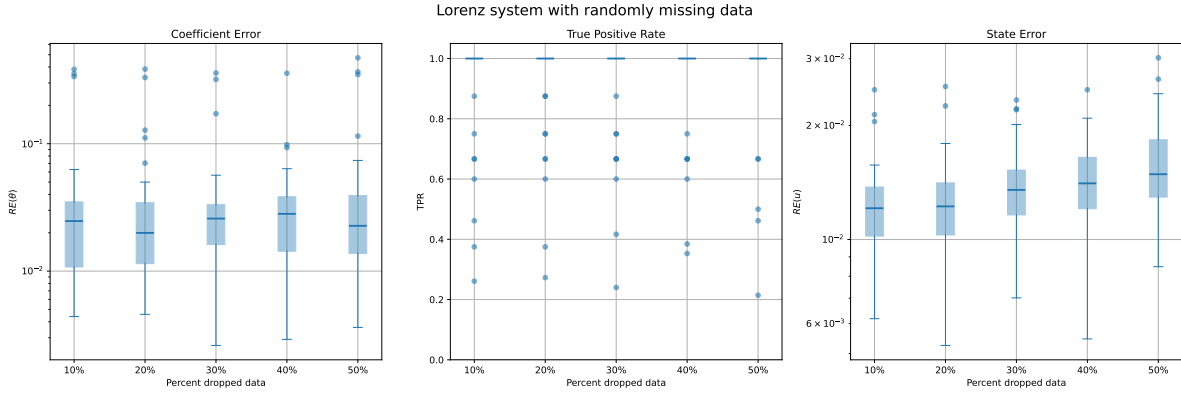


**Figure 9.** Each boxplot summarizes 50 independent noise realizations per noise level for the Lorenz system with various levels of randomly dropped data.

The candidate library consisted of all polynomial terms up to degree 2, so that

$$(5.6) \quad N = \begin{bmatrix} \dot{x}_1 \\ \vdots \\ \dot{x}_5 \end{bmatrix} = \begin{bmatrix} 1 & x_1 & \cdots & x_5 & x_1^2 & x_1x_2 & \cdots & x_5^2 \\ \vdots & \vdots & \vdots & \vdots & \vdots & \vdots & \vdots & \vdots \\ 1 & x_1 & \cdots & x_5 & x_1^2 & x_1x_2 & \cdots & x_5^2 \end{bmatrix} \circ \theta,$$

where  $\theta \in \mathbb{R}^{5 \times 21}$  is a coefficient matrix containing 105 entries.

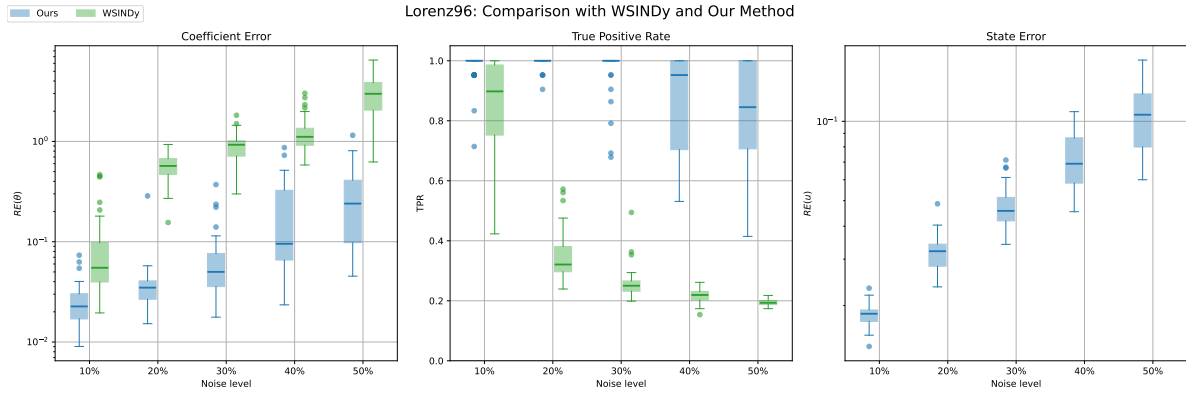


**Figure 10.** Comparison of our algorithm vs. WSINDy. Each boxplot summarizes 50 independent noise realizations per noise level.

We compare our method to WSINDy in figure 10, where we see again the ability of our method to have significantly higher model recovery rates, especially as the level of noise increases. Despite the large candidate library, the median TPR stays above 0.9 for noise levels up to 40%. Figure 11 depicts an example of state reconstruction under 30% noise, along with the corresponding discovered model in (5.7).

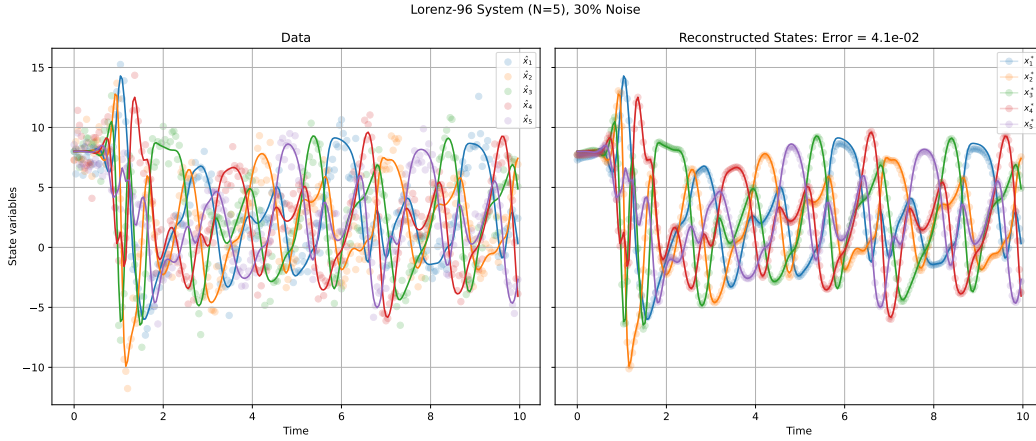


**Figure 11.** Visualization of the Lorenz96 system's components over time. Left: the true state of the system (solid), and observed data (dots); Right: the reconstructed state variables.

$$\begin{aligned}
 \dot{x}_1 &= 8.005 - 0.983x_1 + 1.010x_2x_5 - 1.016x_4x_5 \\
 \dot{x}_2 &= 8.144 - 1.032x_2 + 1.021x_1x_3 - 1.035x_1x_5 \\
 \dot{x}_3 &= 7.840 - 0.954x_3 - 0.999x_1x_2 + 1.017x_2x_4 \\
 \dot{x}_4 &= 8.020 - 1.042x_4 - 1.015x_2x_3 + 1.045x_3x_5 \\
 \dot{x}_5 &= 7.763 - 0.994x_5 + 0.997x_1x_4 - 1.009x_3x_4
 \end{aligned}
 \tag{5.7}$$

**5.4. Nonlinear term libraries and the Colpitts oscillator.** One of the current method's virtues is that candidate models are not required to be linear in parameters, unlike other sparse regression methods that rely on linear least squares. To illustrate this feature, we study the Colpitts oscillator as described in [1] and given by,

$$\begin{aligned}
 \dot{x} &= \alpha_C z \\
 \dot{y} &= \eta(1 - \exp(ax) + z) \\
 \dot{z} &= -\gamma(x + y) - qz.
 \end{aligned}
 \tag{5.8}$$

where the parameter  $a$  in the term  $\exp(ax)$  is also unknown *a priori*. Parameters in this class are estimated in the regression method, although are ignored for purposes of sparsity (the prefactor of such a term, on the other hand, could be set to zero and the term removed if the algorithm permits). Ribera et al. [58] similarly observe that such library terms may be included, and demonstrated successful recovery of this system under noise-free conditions. Our aim here is to show even in the presence of large noise, the correct system can be recovered.

Simulated data used  $(\alpha_C, \eta, \gamma, q, a) = (5, 6.2723, 0.0797, 0.6898, -1)$  and initial condition  $(x_0, y_0, z_0) = (0.01, 0, 0)$ , and were generated for the interval  $t \in (0, 50)$  with sampling rate  $\Delta t = 0.1$ , resulting in a total of 1500 data points across 500 time steps. The initial library

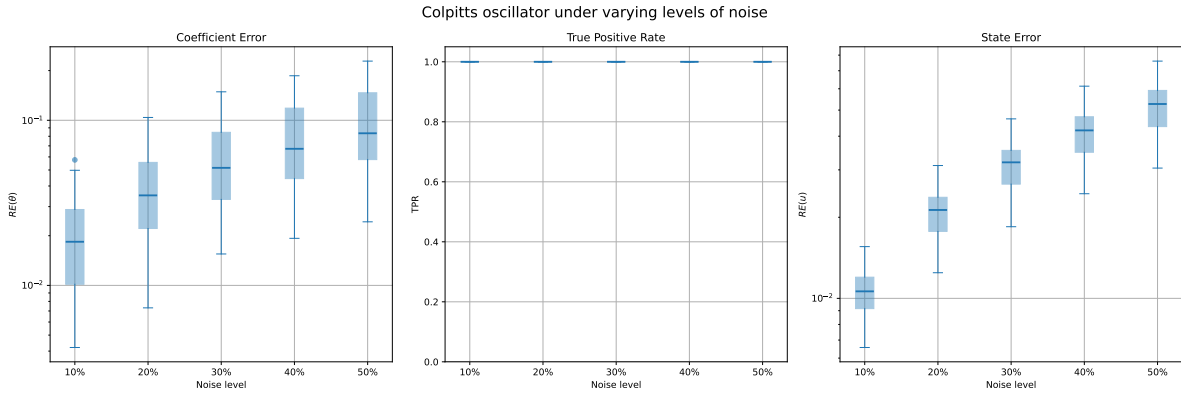


**Figure 12.** Each boxplot summarizes 50 independent noise realizations per noise level. A line at  $TPR = 1$  indicates most realizations achieve perfect recovery.

provided was:

$$N = \begin{bmatrix} \dot{x}_1 \\ \dot{x}_2 \\ \dot{x}_3 \end{bmatrix} = \begin{bmatrix} 1 & x_1 & x_2 & x_3 & x_1x_2 & x_1x_3 & x_2x_3 & x_1^2 & x_2^2 & x_3^2 & e^{ax_1} \\ 1 & x_1 & x_2 & x_3 & x_1x_2 & x_1x_3 & x_2x_3 & x_1^2 & x_2^2 & x_3^2 & e^{ax_1} \\ 1 & x_1 & x_2 & x_3 & x_1x_2 & x_1x_3 & x_2x_3 & x_1^2 & x_2^2 & x_3^2 & e^{ax_1} \end{bmatrix} \odot \theta,$$

where  $\theta \in \mathbb{R}^{3 \times 12}$  is a linear coefficient matrix, thus there are 37 coefficients to optimize over including the nonlinear coefficient  $a$ . Due to the large difference in scales between system components, we normalize the states as  $\bar{x}_i = \hat{x}_i / \text{std}(\hat{x}_i)$  and perform optimization over  $\bar{x}$ . The original system coefficients are then recovered by appropriately rescaling the optimized coefficients.

Figure 13 shows a representative example with 50% noise added with the corresponding discovered equation

$$(5.9) \quad \begin{aligned} \dot{x} &= 5.08z \\ \dot{y} &= 6.68 - 5.75 \exp(-1.01x) + 6.35z \\ \dot{z} &= -0.08x - 0.08y - 0.77z. \end{aligned}$$

Figure 12 summarizes relative errors and true positive rates (TPR) from 50 trials across various noise levels. Notably, our method shows remarkable ability to consistently capture the nonlinear parameter even with substantial noise. These results underscore the potential of our approach when linear libraries are not sufficient in explaining the dynamics.

**5.5. Model Refinement.** While the previous examples focused on recovering governing equations under a fixed discretization, they assume that the data sampling rate was sufficiently fine to capture the essential system dynamics. Here, we relax that assumption and explore how the choice of model-grid spacing interacts with the sampling rate of the data. This experiment serves as a preliminary investigation toward understanding the tradeoff between discretization accuracy and model recovery in our framework.

We performed a study using the Van der Pol and Lorenz systems under 20% measurement noise. Observed data were sampled at fixed intervals of  $\Delta t = 0.05, 0.1, 0.2,$  and  $0.4,$  while the

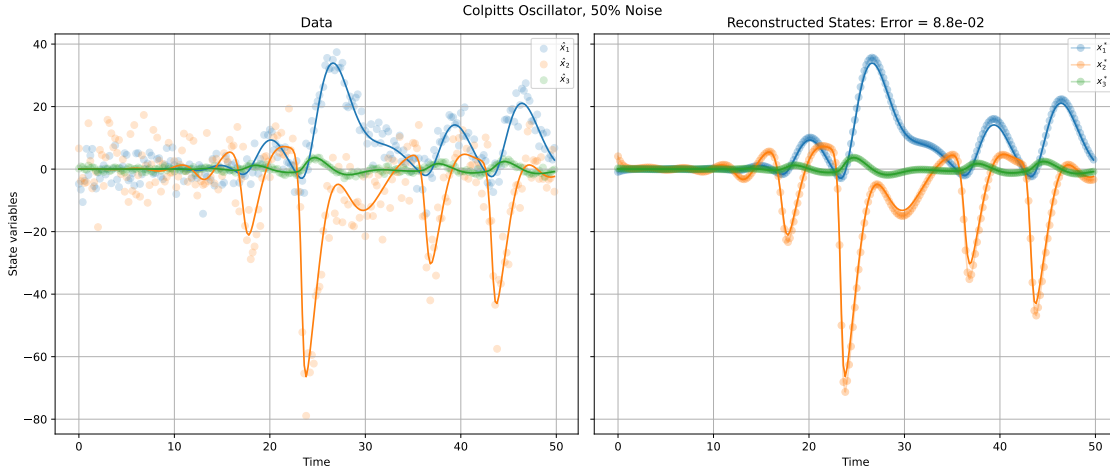


**Figure 13.** Visualization of the Colpitts oscillator’s components over time. Left: the true state of the system (solid), and observed data (dots); Right: the reconstructed state variables.

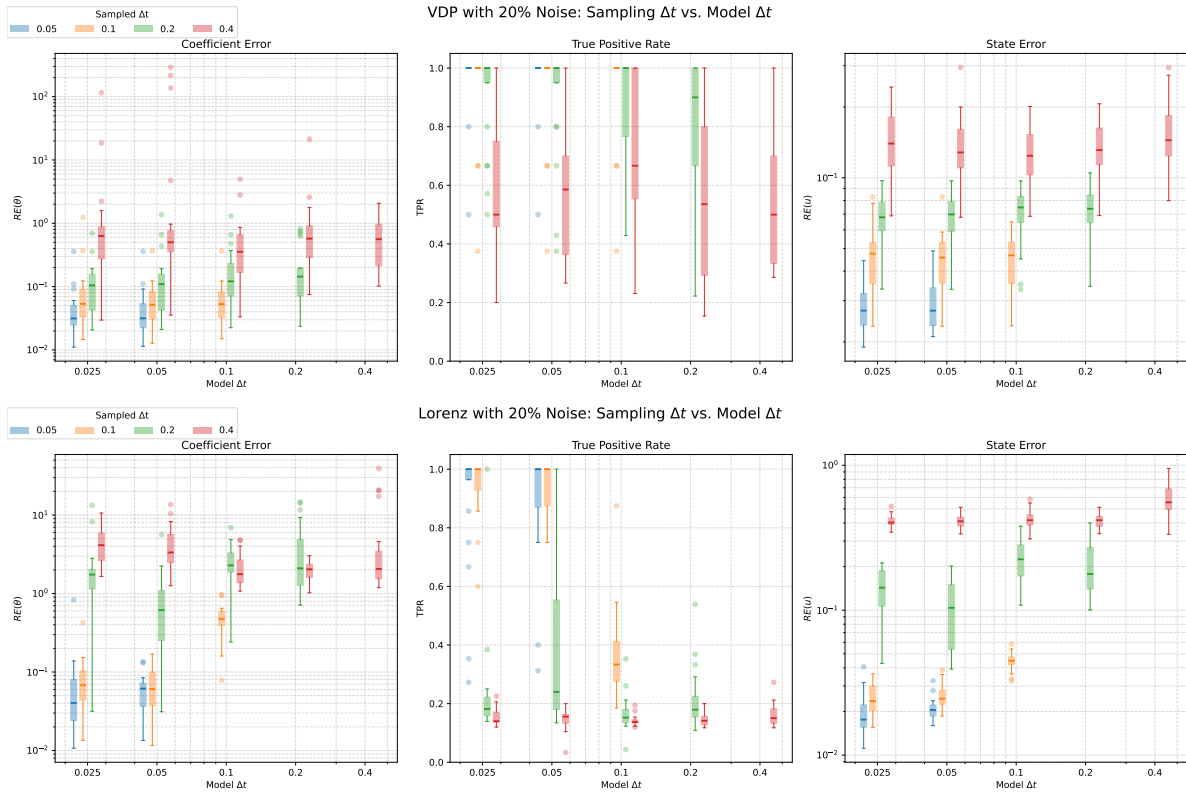
model discretization used for optimization was independently varied between  $\Delta t \in (0.025, 0.4)$ . For each combination of sampling frequency and model grid, the discovery procedure was repeated over 20 independent noise realizations.

Figure 14 shows refinement of the model grid generally improves parameter and state accuracy up to a limit. For the Van der Pol system, moderate refinement yields small but consistent gains, though at the coarsest sampling interval ( $\Delta \hat{t} = 0.4$ ) refinement provides little benefit. For the Lorenz system, refinement leads to significant improvements at finer sampling intervals ( $\Delta \hat{t} \leq 0.1$ ), but when the data are too coarsely sampled ( $\Delta \hat{t} \geq 0.2-0.4$ ), the benefits saturate. Across both systems, excessive refinement occasionally worsens performance due to the introduction of additional optimization variables. The observed interplay provides insights into the balance between discretization bias, conditioning, and information content. We believe further work in establishing model discretization in a rigorous fashion would be a great extension to this work.

**6. Discussion and conclusions.** In this study, we introduced a framework for model discovery that is robust in extreme situations of limited data and substantial noise. With implementation of automatic differentiation, the procedure outlined here can be extended to a wide variety of problems without significant amounts of coding. In addition, local discretization schemes can be implemented that allow for arbitrary accuracy of solution representations, yet provide sparsity of the Hessian required for efficient use of second-order optimization techniques.

Our formulation was chosen to limit the requirement for significant user configuration and manual fine-tuning. This is often a disadvantage of many data-driven algorithms where there is a need to supply numerous hyperparameters, neural architectures, as well as preprocess or filter data. We expect that further improvements could directly integrate hyperparameter selection within the main optimization algorithm.

There are a variety of natural extensions to this work. The abstract setting given in section



**Figure 14.** Effect of model-grid refinement on the Van der Pol system (top) and Lorenz system (bottom) under 20% measurement noise. Boxplots show parameter error ( $RE(\theta)$ ), true positive rate (TPR), and state error ( $RE(u)$ ) as functions of model-grid spacing for different sampling intervals.

2 makes no restriction to ordinary differential equations. We expect that our framework can be adapted to applications such as differential-algebraic systems and partial differential equations, although the latter would entail very high dimensional optimization. We also imagine that merging our ideas with weak-form coarse discretizations might be valuable in situations where fine-scale discretizations lead to computational intractability. Lastly, further improvements in the underlying formulation could allow for hyperparameters to be treated as statistical parameters to be inferred, as in [27].

The sophistication of our methodology is accompanied by its own set of challenges, including a complex optimization landscape and poor conditioning. While the hybrid loss function ameliorates some of the difficulties of non-convexity, there are nonetheless circumstances where undesirable local minima are encountered. Further improvement of the optimization algorithms required here should be pursued, and will most likely require novel or bespoke methods.

**Acknowledgments.** The authors were supported through NSF awards DMS-1908968 and DMS-2407033. Additionally, TM was supported by the Department of Defense (DoD) through the National Defense Science & Engineering Graduate (NDSEG) Fellowship Program.

## REFERENCES

- [1] H. ABARBANEL, *Predicting the future: Completing models of observed complex systems*, Understanding complex systems, Springer, New York, NY, 2013 ed., June 2013.
- [2] A. S. ACKLEH, R. R. FERDINAND, AND S. REICH, *Numerical studies of parameter estimation techniques for nonlinear evolution equations*, *Kybernetika*, 34 (1998), pp. 693–712.
- [3] H. AKAIKE, *Information theory and an extension of the maximum likelihood principle*, in *Selected Papers of Hirotugu Akaike*, E. Parzen, K. Tanabe, and G. Kitagawa, eds., Springer New York, New York, NY, 1998, pp. 199–213.
- [4] M. ASHYRALIYEV, J. JAEGER, AND J. G. BLOM, *Parameter estimation and determinability analysis applied to drosophila gap gene circuits*, *BMC Systems Biology*, 2 (2008), p. 83.
- [5] S. ATKINSON, W. SUBBER, L. WANG, G. KHAN, P. HAWI, AND R. GHANEM, *Data-driven discovery of free-form governing differential equations*, arXiv preprint arXiv:1910.05117, (2019).
- [6] D. A. BARAJAS-SOLANO AND A. M. TARTAKOVSKY, *Approximate bayesian model inversion for pdes with heterogeneous and state-dependent coefficients*, *Journal of Computational Physics*, 395 (2019), pp. 247–262.
- [7] J. BERG AND K. NYSTRÖM, *Neural network augmented inverse problems for pdes*, arXiv preprint arXiv:1712.09685, (2017).
- [8] H. G. BOCK, *Recent advances in parameter identification techniques for ode*, in *Numerical Treatment of Inverse Problems in Differential and Integral Equations: Proceedings of an International Workshop*, Heidelberg, Fed. Rep. of Germany, August 30–September 3, 1982, Springer, 1983, pp. 95–121.
- [9] J. BONGARD AND H. LIPSON, *Automated reverse engineering of nonlinear dynamical systems*, *Proceedings of the National Academy of Sciences*, 104 (2007), pp. 9943–9948.
- [10] C. BONNEVILLE AND C. EARLS, *Bayesian deep learning for partial differential equation parameter discovery with sparse and noisy data*, *Journal of Computational Physics: X*, 16 (2022), p. 100115.
- [11] G.-J. BOTH, S. CHOUDHURY, P. SENS, AND R. KUSTERS, *Deepmod: Deep learning for model discovery in noisy data*, *Journal of Computational Physics*, 428 (2021), p. 109985.
- [12] N. J. BRUNEL, *Parameter estimation of ode's via nonparametric estimators*, *Electronic Journal of Statistics*, 2 (2008), pp. 1242–1267.
- [13] S. L. BRUNTON, J. L. PROCTOR, AND J. N. KUTZ, *Discovering governing equations from data by sparse identification of nonlinear dynamical systems*, *Proceedings of the national academy of sciences*, 113 (2016), pp. 3932–3937.
- [14] Y. CHEN, Y. LUO, Q. LIU, H. XU, AND D. ZHANG, *Symbolic genetic algorithm for discovering open-form partial differential equations (sga-pde)*, *Physical Review Research*, 4 (2022), p. 023174.
- [15] T. F. COLEMAN AND J. J. MORÉ, *Estimation of sparse hessian matrices and graph coloring problems*, *Math. Program.*, 28 (1984), pp. 243–270.
- [16] W. CROFT, C. M. ELLIOTT, G. LADDS, B. STINNER, C. VENKATARAMAN, AND C. WESTON, *Parameter identification problems in the modelling of cell motility*, *Journal of mathematical biology*, 71 (2015), pp. 399–436.
- [17] C. B. DELAHUNT AND J. N. KUTZ, *A toolkit for data-driven discovery of governing equations in high-noise regimes*, *IEEE Access*, 10 (2022), pp. 31210–31234.
- [18] M. A. DEWAR, V. KADIRKAMANATHAN, M. OPPER, AND G. SANGUINETTI, *Parameter estimation and inference for stochastic reaction-diffusion systems: application to morphogenesis in d. melanogaster*, *BMC Systems Biology*, 4 (2010), p. 21.
- [19] G. EVENSEN, *Data assimilation: The ensemble kalman filter. 2007*.
- [20] U. FASEL, J. N. KUTZ, B. W. BRUNTON, AND S. L. BRUNTON, *Ensemble-sindy: Robust sparse model discovery in the low-data, high-noise limit, with active learning and control*, *Proceedings of the Royal Society A*, 478 (2022), p. 20210904.
- [21] R. FLETCHER AND C. M. REEVES, *Function minimization by conjugate gradients*, *Comput. J.*, 7 (1964), pp. 149–154.
- [22] J. FULLANA, P. LE GAL, M. ROSSI, AND S. ZALESKI, *Identification of parameters in amplitude equations describing coupled wakes*, *Physica D: Nonlinear Phenomena*, 102 (1997), pp. 37–56.
- [23] N. GALIOTO AND A. A. GORODETSKY, *Bayesian system id: optimal management of parameter, model, and measurement uncertainty*, *Nonlinear Dynamics*, 102 (2020), pp. 241–267.

- [24] M. R. GARVIE, P. K. MAINI, AND C. TRENCHIA, *An efficient and robust numerical algorithm for estimating parameters in Turing systems*, Journal of Computational Physics, 229 (2010), pp. 7058–7071.
- [25] A. H. GEBREMEDHIN, F. MANNE, AND A. POTHEN, *What color is your jacobian? graph coloring for computing derivatives*, SIAM Rev., 47 (2005), pp. 629–705.
- [26] K. GLASNER, *Optimization algorithms for parameter identification in parabolic partial differential equations*, Computational and Applied Mathematics, 40 (2021), p. 146.
- [27] K. GLASNER, *Data-driven learning of differential equations: combining data and model uncertainty*, Computational and Applied Mathematics, 42 (2023), p. 36.
- [28] S. GUGUSHVILI AND C. A. KLAASSEN,  *$\sqrt{n}$ -consistent parameter estimation for systems of ordinary differential equations: bypassing numerical integration via smoothing*, Bernoulli, 18 (2012), pp. 1061–1098.
- [29] M. HARING, E. I. GROTLI, S. RIEMER-SORENSEN, K. SEEL, AND K. G. HANSEN, *A levenberg-marquardt algorithm for sparse identification of dynamical systems*, IEEE Transactions on Neural Networks and Learning Systems, (2022).
- [30] S. M. HIRSH, D. A. BARAJAS-SOLANO, AND J. N. KUTZ, *Sparsifying priors for bayesian uncertainty quantification in model discovery*, Royal Society Open Science, 9 (2022), p. 211823.
- [31] B. JIN AND P. MAASS, *Sparsity regularization for parameter identification problems*, Inverse Problems, 28 (2012), p. 123001.
- [32] G. E. KARNIADAKIS, I. G. KEVREKIDIS, L. LU, P. PERDIKARIS, S. WANG, AND L. YANG, *Physics-informed machine learning*, Nature Reviews Physics, 3 (2021), pp. 422–440.
- [33] E. KIYANI, S. SILBER, M. KOOSHKBAGHI, AND M. KARTTUNEN, *Machine-learning-based data-driven discovery of nonlinear phase-field dynamics*, Physical Review E, 106 (2022), p. 065303.
- [34] J. H. LAGERGREN, J. T. NARDINI, G. MICHAEL LAVIGNE, E. M. RUTTER, AND K. B. FLORES, *Learning partial differential equations for biological transport models from noisy spatio-temporal data*, Proceedings of the Royal Society A: Mathematical, Physical and Engineering Sciences, 476 (2020), p. 20190800, <https://doi.org/10.1098/rspa.2019.0800>, <https://royalsocietypublishing.org/doi/abs/10.1098/rspa.2019.0800>, <https://arxiv.org/abs/https://royalsocietypublishing.org/doi/pdf/10.1098/rspa.2019.0800>.
- [35] K. LEVENBERG, *A method for the solution of certain non-linear problems in least squares*, Quart. Appl. Math., 2 (1944), pp. 164–168.
- [36] H. LIANG AND H. WU, *Parameter estimation for differential equation models using a framework of measurement error in regression models*, Journal of the American Statistical Association, 103 (2008), pp. 1570–1583.
- [37] D. C. LIU AND J. NOCEDAL, *On the limited memory bfgs method for large scale optimization*, Math. Program., 45 (1989), pp. 503–528.
- [38] Z. LONG, Y. LU, AND B. DONG, *Pde-net 2.0: Learning pdes from data with a numeric-symbolic hybrid deep network*, Journal of Computational Physics, 399 (2019), p. 108925.
- [39] E. LORENZ, *Predictability: a problem partly solved*, PhD thesis, Shinfield Park, Reading, 1995 1995.
- [40] E. N. LORENZ, *Deterministic nonperiodic flow*, J. Atmos. Sci., 20 (1963), pp. 130–141.
- [41] N. M. MANGAN, J. N. KUTZ, S. L. BRUNTON, AND J. L. PROCTOR, *Model selection for dynamical systems via sparse regression and information criteria*, Proceedings of the Royal Society A: Mathematical, Physical and Engineering Sciences, 473 (2017), p. 20170009.
- [42] D. W. MARQUARDT, *An algorithm for least-squares estimation of nonlinear parameters*, Journal of the Society for Industrial and Applied Mathematics, 11 (1963), pp. 431–441.
- [43] M. MASLYAEV, A. HVATOV, AND A. V. KALYUZHAYA, *Partial differential equations discovery with epde framework: Application for real and synthetic data*, Journal of Computational Science, 53 (2021), p. 101345.
- [44] D. A. MESSENGER AND D. M. BORTZ, *Weak sindy for partial differential equations*, Journal of Computational Physics, 443 (2021), p. 110525.
- [45] D. A. MESSENGER AND D. M. BORTZ, *Weak sindy: Galerkin-based data-driven model selection*, Multiscale Modeling & Simulation, 19 (2021), pp. 1474–1497.
- [46] H. MOHIMANI, M. BABAIE-ZADEH, AND C. JUTTEN, *A Fast Approach for Overcomplete Sparse Decomposition Based on Smoothed  $l^0$  Norm*, IEEE Transactions on Signal Processing, 57 (2009), pp. 289–301, <https://doi.org/10.1109/TSP.2008.2007606>. Conference Name: IEEE Transactions on Signal Pro-

- cessing.
- [47] D. NGUYEN, S. OUALA, L. DRUMETZ, AND R. FABLET, *Assimilation-based learning of chaotic dynamical systems from noisy and partial data*, in ICASSP 2020-2020 IEEE International Conference on Acoustics, Speech and Signal Processing (ICASSP), IEEE, 2020, pp. 3862–3866.
  - [48] J. NOCEDAL AND S. WRIGHT, *Numerical optimization*, Springer Series in Operations Research and Financial Engineering, Springer Nature, 2006.
  - [49] M. J. D. POWELL AND P. L. TOINT, *On the estimation of sparse hessian matrices*, SIAM J. Numer. Anal., 16 (1979), pp. 1060–1074.
  - [50] M. RAISSI AND G. E. KARNIADAKIS, *Hidden physics models: Machine learning of nonlinear partial differential equations*, Journal of Computational Physics, 357 (2018), pp. 125–141.
  - [51] M. RAISSI, P. PERDIKARIS, AND G. E. KARNIADAKIS, *Machine learning of linear differential equations using gaussian processes*, Journal of Computational Physics, 348 (2017), pp. 683–693.
  - [52] M. RAISSI, P. PERDIKARIS, AND G. E. KARNIADAKIS, *Physics-informed neural networks: A deep learning framework for solving forward and inverse problems involving nonlinear partial differential equations*, Journal of Computational physics, 378 (2019), pp. 686–707.
  - [53] J. RAMSAY AND G. HOOKER, *Dynamic data analysis*, Springer, 2017.
  - [54] J. O. RAMSAY, G. HOOKER, D. CAMPBELL, AND J. CAO, *Parameter estimation for differential equations: a generalized smoothing approach*, Journal of the Royal Statistical Society: Series B (Statistical Methodology), 69 (2007), pp. 741–796.
  - [55] J. O. RAMSAY AND B. W. SILVERMAN, *Fitting differential equations to functional data: Principal differential analysis*, Springer, 2005.
  - [56] P. A. REINBOLD, D. R. GUREVICH, AND R. O. GRIGORIEV, *Using noisy or incomplete data to discover models of spatiotemporal dynamics*, Physical Review E, 101 (2020), p. 010203.
  - [57] A. RETZLER, J. SWEVERS, J. GILLIS, AND Z. KOLLÁR, *Shooting methods for identification of nonlinear state-space grey-box models*, in 2022 IEEE 17th International Conference on Advanced Motion Control (AMC), IEEE, 2022, pp. 207–212.
  - [58] H. RIBERA, S. SHIRMAN, A. NGUYEN, AND N. MANGAN, *Model selection of chaotic systems from data with hidden variables using sparse data assimilation*, Chaos: An Interdisciplinary Journal of Nonlinear Science, 32 (2022).
  - [59] S. H. RUDY, S. L. BRUNTON, J. L. PROCTOR, AND J. N. KUTZ, *Data-driven discovery of partial differential equations*, Science Advances, 3 (2017), p. e1602614.
  - [60] H. SCHAEFFER, *Learning partial differential equations via data discovery and sparse optimization*, Proceedings of the Royal Society A: Mathematical, Physical and Engineering Sciences, 473 (2017), p. 20160446.
  - [61] H. SCHAEFFER AND S. G. MCCALLA, *Sparse model selection via integral terms*, Physical Review E, 96 (2017), p. 023302.
  - [62] M. SCHMIDT AND H. LIPSON, *Distilling free-form natural laws from experimental data*, science, 324 (2009), pp. 81–85.
  - [63] G. SCHWARZ, *Estimating the dimension of a model*, aos, 6 (1978), pp. 461–464.
  - [64] I. SGURA, A. S. LAWLESS, AND B. BOZZINI, *Parameter estimation for a morphochemical reaction-diffusion model of electrochemical pattern formation*, Inverse Problems in Science and Engineering, 27 (2019), pp. 618–647.
  - [65] T. STEIHAUG, *The conjugate gradient method and trust regions in large scale optimization*, SIAM J. Numer. Anal., 20 (1983), pp. 626–637.
  - [66] R. STEPHANY AND C. EARLS, *Pde-learn: Using deep learning to discover partial differential equations from noisy, limited data*, arXiv preprint arXiv:2212.04971, (2022).
  - [67] R. STEPHANY AND C. EARLS, *Pde-read: Human-readable partial differential equation discovery using deep learning*, Neural Networks, 154 (2022), pp. 360–382.
  - [68] M. TANG, W. LIAO, R. KUSKE, AND S. H. KANG, *Weakident: Weak formulation for identifying differential equation using narrow-fit and trimming*, Journal of Computational Physics, 483 (2023), p. 112069.
  - [69] S.-M. UDRESCU AND M. TEGMARK, *Ai feynman: A physics-inspired method for symbolic regression*, Science Advances, 6 (2020), p. eaay2631.
  - [70] H. U. VOSS, J. TIMMER, AND J. KURTHS, *Nonlinear dynamical system identification from uncertain and indirect measurements*, International Journal of Bifurcation and Chaos, 14 (2004), pp. 1905–1933.

- [71] J. WENTZ AND A. DOOSTAN, *Derivative-based sindy (dsindy): Addressing the challenge of discovering governing equations from noisy data*, Computer Methods in Applied Mechanics and Engineering, 413 (2023), p. 116096.
- [72] H. XU, D. ZHANG, AND J. ZENG, *Deep-learning of parametric partial differential equations from sparse and noisy data*, Physics of Fluids, 33 (2021), p. 037132.
- [73] J. YE, N. KADAKIA, P. J. ROZDEBA, H. D. ABARBANEL, AND J. C. QUINN, *Improved variational methods in statistical data assimilation*, Nonlinear Processes in Geophysics, 22 (2015), pp. 205–213.
- [74] N. YOSHINAGA AND S. TOKUDA, *Bayesian modelling of pattern formation from one snapshot of pattern*, arXiv preprint arXiv:2006.06125, (2020).
- [75] T. ZHANG, G. LIU, L. WANG, AND Z.-R. LU, *Adaptive integral alternating minimization method for robust learning of nonlinear dynamical systems from highly corrupted data*, Chaos: An Interdisciplinary Journal of Nonlinear Science, 33 (2023).
- [76] H. ZHAO, R. D. BRAATZ, AND M. Z. BAZANT, *Image inversion and uncertainty quantification for constitutive laws of pattern formation*, Journal of Computational Physics, 436 (2021), p. 110279.
- [77] H. ZHAO, B. D. STOREY, R. D. BRAATZ, AND M. Z. BAZANT, *Learning the physics of pattern formation from images*, Physical Review Letters, 124 (2020), p. 060201.
- [78] J. ZHUANG, T. TANG, Y. DING, S. C. TATIKONDA, N. DVORNEK, X. PAPADEMETRIS, AND J. DUNCAN, *Adabelief optimizer: Adapting stepsizes by the belief in observed gradients*, in Advances in Neural Information Processing Systems, H. Larochelle, M. Ranzato, R. Hadsell, M. Balcan, and H. Lin, eds., vol. 33, Curran Associates, Inc., 2020, pp. 18795–18806, [https://proceedings.neurips.cc/paper\\_files/paper/2020/file/d9d4f495e875a2e075a1a4a6e1b9770f-Paper.pdf](https://proceedings.neurips.cc/paper_files/paper/2020/file/d9d4f495e875a2e075a1a4a6e1b9770f-Paper.pdf).

**Appendix A. Insufficient Candidate Libraries.** A sufficiently expressive candidate library is essential for accurately recovering the underlying dynamics of a system. Here, we illustrate the result of using an insufficient library by applying our method to the Van der Pol oscillator with a basis limited to polynomials of degree at most two, thereby omitting its characteristic cubic term (see (A.1)).

The data generation setup follows that of section 5.1, with a time step of  $dt = 0.04$ , resulting in 201 time steps and a total of 402 data points. For model selection, we perform a grid search over the regularization parameters  $(\lambda, R) = (10^i, 10^j)$  with  $i \in \{-3, -2, \dots, 3\}$  and  $j \in \{-4, -3, \dots, 0\}$ , resulting in 35 candidate models, of which the winning model is shown in table 1.

Among these, only three distinct model structures were present. For each structure, we retained the model with the lowest validation error. The recovered models are summarized in table 1 and visualized in figure 15. As expected, we observe a clear relationship between the regularization parameter  $\lambda$  and model error: larger values of  $\lambda$  correspond to higher model errors. We see here that our method selects that which is close to the data, but results in large model error. Models selected with smaller  $\lambda$  values tend to result in lower model error and in turn appear smoother. This trade-off highlights a strength of our framework as it offers interpretable options, enabling experts to balance fidelity to data against model simplicity depending on the specific needs of the application.

$$(A.1) \quad N = \begin{bmatrix} \dot{x}_1 \\ \dot{x}_2 \end{bmatrix} - \begin{bmatrix} x_1 & x_2 & x_1 x_2 & x_1^2 & x_2^2 \\ x_1 & x_2 & x_1 x_2 & x_1^2 & x_2^2 \end{bmatrix} \circ \theta,$$

Rank	$\lambda$	$R$	Val. Err	Model Err	State Err	Model Discovered
1	$10^2$	$10^{-4}$	$1.13 \times 10^{-1}$	3.75	$5.77 \times 10^{-2}$	$\dot{x}_1 = 1.063 x_2$ $\dot{x}_2 = -0.993 x_1$
2	$10^0$	$10^{-4}$	$3.75 \times 10^{-1}$	$5.58 \times 10^{-2}$	$3.39 \times 10^{-1}$	$\dot{x}_1 = 0.997 x_2$ $\dot{x}_2 = -0.772 x_1 - 0.297 x_1 x_2$
3	$10^{-1}$	$10^{-4}$	$4.80 \times 10^{-1}$	$9.67 \times 10^{-4}$	$4.42 \times 10^{-1}$	$\dot{x}_1 = 1.007 x_2$ $\dot{x}_2 = -0.764 x_1 - 0.071 x_1^2 - 0.361 x_1 x_2 + 0.072 x_2^2$

Table 1

Discovered models at various  $\lambda$  and  $R$  values. Each balances model complexity with accuracy, offering candidates that users may select based on application-specific trade-offs.

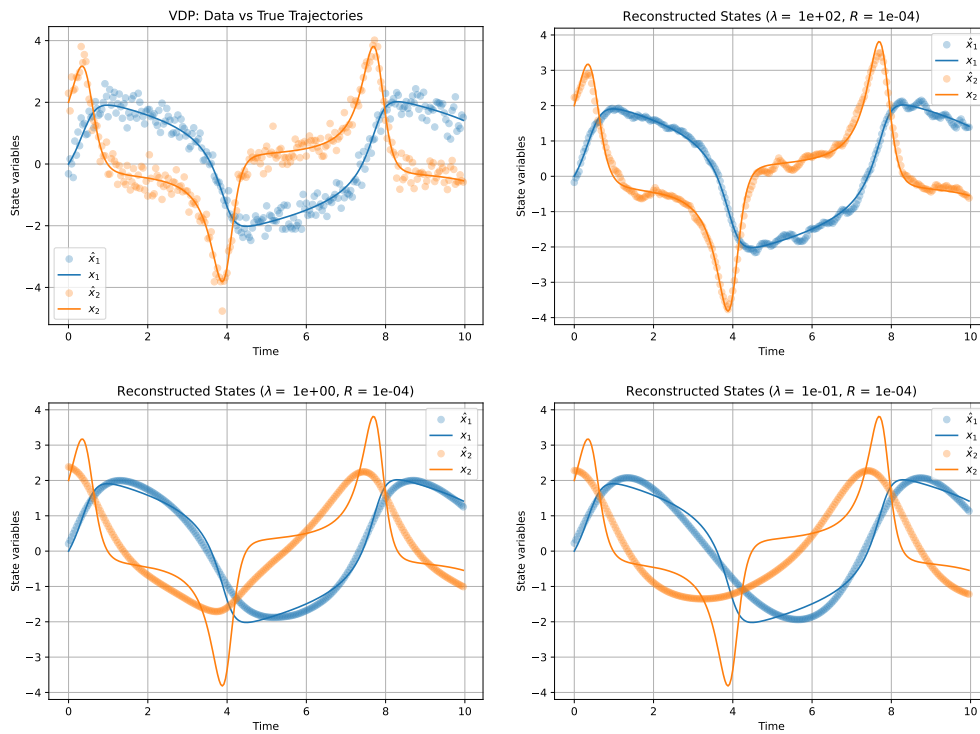


Figure 15. State estimation using recovered models for the Van der Pol oscillator using an insufficient library of polynomial terms (up to degree 2).

## Appendix B. Levenberg-Marquardt.

**Algorithm B.1** Levenberg-Marquardt Optimization

---

```

1: procedure LEVENBERGMARQUARDT( $f, \nabla f, \nabla^2 f, \mathbf{x}, \alpha, \tau, \epsilon$ )
2:   Initialize  $\alpha, \tau_1, \tau_2$  ▷ e.g.,  $\alpha = 1, \tau_1 = 0.25, \tau_2 = 2.0$ 
3:   while  $\|g\| > \epsilon$  do
4:      $g \leftarrow \nabla f(\mathbf{x}), \quad H_\alpha \leftarrow \nabla^2 f(\mathbf{x}) + \alpha I$  ▷ Gradient and modified Hessian
5:     Solve  $H_\alpha d = -g$ 
6:      $f_{\text{old}}, f_{\text{test}} \leftarrow f(\mathbf{x}), f(\mathbf{x} + d)$ 
7:     predicted  $\leftarrow -g^T d - \frac{1}{2} d^T H d$  ▷ Predicted decrease
8:      $\rho \leftarrow (f_{\text{old}} - f_{\text{test}}) / \text{predicted}$  ▷ Agreement with model
9:     if  $f_{\text{test}} < f_{\text{old}}$  then
10:       $\mathbf{x} \leftarrow \mathbf{x} + d$  ▷ Accept step
11:      if  $\rho < 0.25$  then
12:         $\alpha \leftarrow \min(\alpha \cdot \tau_2, \alpha_{\text{max}})$  ▷ Bad agreement, increase  $\alpha$ 
13:      else if  $\rho > 0.75$  then
14:         $\alpha \leftarrow \max(\alpha \cdot \tau_1, \alpha_{\text{min}})$  ▷ Good agreement, decrease  $\alpha$ 
15:      else
16:         $\alpha \leftarrow \min(\alpha \cdot \tau_2, \alpha_{\text{max}})$  ▷ Reject step, increase  $\alpha$ 
return  $\mathbf{x}$ 

```

---